Serum metabolic fingerprints encode functional biomarkers for ovarian cancer diagnosis: a large-scale cohort study

Wanshan Liu,[a,b,c,d,f] Xiaoxiao Hu,[a,b,f] Zhouzhou Bao,[a,b,f] Yanyan Li,[a,b,c,d] Juxiang Zhang,[a,b,c,d] Shouzhi Yang,[a,b,c,d] Yida Huang,[a,b,c,d] Ruimin Wang,[a,b,c,d] Jiao Wu,[a,b,c,d] Xiaoyu Xu,[a,b,c,d] Qi Sang,[a,b,c,d] Wen Di,[a,b,****] Huaiwu Lu,[e,***] Xia Yin,[a,b,**] and Kun Qian[a,b,c,d,*]

[a]Department of Obstetrics and Gynecology, Renji Hospital, School of Medicine, Shanghai Jiao Tong University, Shanghai 200127, PR China
[b]State Key Laboratory for Oncogenes and Related Genes, Shanghai Key Laboratory of Gynecologic Oncology, Shanghai 200127, PR China
[c]State Key Laboratory of Systems Medicine for Cancer, School of Biomedical Engineering, Institute of Medical Robotics and Shanghai Academy of Experimental Medicine, Shanghai Jiao Tong University, Shanghai 200030, PR China
[d]Division of Cardiology, Renji Hospital, School of Medicine, Shanghai Jiao Tong University, Shanghai 200127, PR China
[e]Department of Gynecologic Oncology, Sun Yat-Sen Memorial Hospital, Sun Yat-Sen University, Guangzhou 510120, PR China

eBioMedicine
2025;115: 105706
Published Online xxx
https://doi.org/10.1016/j.ebiom.2025.105706

Summary

Background Ovarian cancer (OC) ranks as the most lethal gynaecological malignancy worldwide, with early diagnosis being crucial yet challenging. Current diagnostic methods like transvaginal ultrasound and blood biomarkers show limited sensitivity/specificity. This study aimed to identify and validate serum metabolic biomarkers for OC diagnosis using the largest cohort reported to date.

Methods We constructed a large-scale OC-associated cohort of 1432 subjects, including 662 OC, 563 benign ovarian disease, and 207 healthy control subjects, across retrospective (n = 1073) and set-aside validation (n = 359) cohorts. Serum metabolic fingerprints (SMFs) were recorded using nanoparticle-enhanced laser desorption/ionization mass spectrometry (NELDI-MS). A diagnostic panel was developed through machine learning of SMFs in the discovery cohort and validated in independent verification and set-aside validation cohorts. The identified metabolic biomarkers were further validated using liquid chromatography MS and their biological functions were assessed in OC cell lines.

Findings We identified a metabolic biomarker panel including glucose, histidine, pyrrole-2-carboxylic acid, and dihydrothymine. This panel achieved consistent areas under the curve (AUCs) of 0.87–0.89 for distinguishing between malignant and benign ovarian masses across all cohorts, and improved to AUCs of 0.95–0.99 when combined with risk of ovarian malignancy algorithm (ROMA). In vitro validation provided initial biological context for the metabolic alterations observed in our diagnostic panel.

Interpretation Our study established a reliable serum metabolic biomarker panel for OC diagnosis with potential clinical translations. The NELDI-MS based approach offers advantages of fast analytical speed (~30 s/sample) and low cost (~2–3 dollars/sample), making it suitable for large-scale clinical applications.

Funding MOST (2021YFA0910100), NSFC (82421001, 823B2050, 824B2059, and 82173077), Medical-Engineering Joint Funds of Shanghai Jiao Tong University (YG2021GD02, YG2024ZD07, and YG2023ZD08), Shanghai Science and Technology Committee Project (23JC1403000), Shanghai Institutions of Higher Learning (2021-01-07-00-02-E00083), Shanghai Jiao Tong University Inner Mongolia Research Institute (2022XYJG0001-01-16), Sichuan Provincial Department of Science and Technology (2024YFHZ0176), Innovation Research Plan by the Shanghai Municipal Education Commission (ZXWF082101), Innovative Research Team of High-Level Local Universities in Shanghai (SHSMU-ZDCX20210700), Basic-Clinical Collaborative Innovation Project from Shanghai Immune Therapy Institute, Guangdong Basic and Applied Basic Research Foundation (2024A1515013255).

*Corresponding author. Department of Obstetrics and Gynecology, Renji Hospital, School of Medicine, Shanghai Jiao Tong University, Shanghai 200127, PR China.
**Corresponding author. Department of Obstetrics and Gynecology, Renji Hospital, School of Medicine, Shanghai Jiao Tong University, Shanghai 200127, PR China.
***Corresponding author.
****Corresponding author. Department of Obstetrics and Gynecology, Renji Hospital, School of Medicine, Shanghai Jiao Tong University, Shanghai 200127, PR China.
E-mail addresses: k.qian@sjtu.edu.cn (K. Qian), yinxia@renji.com (X. Yin), luhuaiwu@mail.sysu.edu.cn (H. Lu), diwen@renji.com (W. Di).
[f]These authors contributed equally to this work.

Keywords: Ovarian cancer; Metabolomics; Biomarker; Diagnosis; Machine learning

Research in context

Evidence before this study

Ovarian cancer (OC) is the most lethal gynaecological malignancy globally, causing over 300,000 new cases and 200,000 deaths annually, with early diagnosis being crucial for survival (70–90% for early-stage vs. 15–40% for late-stage).

Current diagnostic methods have limitations: transvaginal ultrasound relies on experienced clinicians with limited sensitivity/specificity (~55–85%), biopsy is invasive with potential risks, and blood biomarkers show suboptimal sensitivity/specificity (~50–70%).

While metabolic biomarkers in blood have shown promise for OC diagnosis, current studies are limited by relatively small-scale cohorts (~200–500), traditional analytical techniques, and lack of biological functional assays.

Added value of this study

We constructed the largest OC-associated cohort to date (1432 subjects) for serum metabolic biomarker discovery and validation.

Using advanced nanoparticle-enhanced laser desorption/ionization mass spectrometry (NELDI-MS), we developed a rapid, cost-effective approach for serum metabolic fingerprints (SMFs).

We identified and validated a metabolic biomarker panel for distinguishing between malignant and benign ovarian masses, and demonstrated initial biological context in OC cell.

Implications of all the available evidence

The identified metabolic biomarker panel provides a promising approach for OC diagnosis with advantages in analytical speed and cost-effectiveness, potentially improving differentiation between malignant and benign ovarian masses.

Introduction

Ovarian cancer (OC) ranks the most lethal gynaecological malignancy globally, accounting for over 300,000 new cases and 200,000 deaths annually.[1,2] ~90% of OC is of epithelial origin, including serous, clear cell, endometrioid, and mucinous subtypes, while the remaining 10% consist of non-epithelial tumours, primarily germ cell and sex cord-stromal tumours.[3] Timely differentiation of OC and Non-OC (especially benign ovarian disease) is important to improve patient outcomes, considering that the 5-year survival rate is 70–90% for early-stage patients (stage I-II), compared with 15–40% for stage III-IV.[4,5] However, current methods for OC diagnosis like transvaginal ultrasound and biopsy rely on experienced clinicians with limited performance (~55–85% sensitivity/specificity for transvaginal ultrasound) or invasive procedures (tissue sampling for biopsy with potential risks).[6–8] Furthermore, the existing blood biomarkers like cancer antigen 125 (CA-125) and human epididymis protein 4 (HE-4) for OC diagnosis are limited by its suboptimal sensitivity/specificity (~50–70%), especially for early-stage patients (~50–60%).[7,9–12] Consequently, over 70% of OC patients are diagnosed after the cancer has metastasized regionally or distantly.[13] The lack of effective tools has significant economic implications, as average treatment cost can reach 80,000 dollars in the first year, potentially increasing to 100,000 dollars in the final year.[14] Therefore, it is urgent to further explore blood-based biomarkers for early diagnosis of OC in clinical settings.

The potential of blood-based biomarkers for early cancer diagnosis has gained increasing recognition, focussing on genes, proteins, and metabolites.[15,16] Proteomic analysis has provided valuable insights into molecular mechanisms underlying OC progression and therapeutic responses.[17,18] Notably, metabolic biomarkers provide a more immediate reflection of disease phenotype and hold the potential to predict the onset of cancers characterized by metabolic reprogramming.[19,20] However, current studies on metabolic biomarkers in blood for OC diagnosis are limited by relatively small-scale cohorts (sample sizes of ~200–500), traditional analytical techniques, and lack of biological functional assays.[10,21–25] Thus, there is a critical need to identify metabolic biomarkers in blood based on a large-scale OC cohort with advanced analytical techniques and validate its biological function for potential diagnostic purposes.

Mass spectrometry (MS) serves as the primary analytical tool for metabolic profiling, owing to its high sensitivity and label-free identification through accurate measurement of mass-to-charge ratio (m/z).[26,27] However, analysis of metabolites in bio-fluids using liquid/gas chromatography MS (LC/GC-MS) showed limited analytical speed and capacity, requiring sample treatment like deproteinization and chromatography for metabolite purification.[28,29] Notably, nanoparticle-enhanced laser desorption/ionization MS (NELDI-MS) with designed ferric oxide nanoparticles enables direct detection of metabolites in bio-fluids containing high levels of salts and proteins, offering enhanced analytical speed and capacity.[30–32] The NELDI-MS recording of serum metabolic fingerprints (SMFs) has shown potential in several diseases and is promising in OC

diagnosis.[32–34] Furthermore, machine learning is instrumental in linking the extensive data in SMFs with clinical outcomes.

In this study, we constructed the largest OC-associated cohort reported to date to validate the serum metabolic biomarkers for diagnosis, through analysis of SMFs recorded by NELDI-MS. Firstly, we constructed a large-scale OC-associated SMFs database of 662 OC, 563 benign ovarian disease, and 207 healthy control subjects using NELDI-MS, comprising 1073 subjects in retrospective cohort and 359 subjects in set-aside validation cohort. Then, we identified a metabolic biomarker panel, including glucose, histidine, pyrrole-2-carboxylic acid (PCA), and dihydrothymine, through machine learning of SMFs. This panel achieved consistent areas under the curve (AUCs) of 0.87–0.89 for distinguishing between malignant and benign ovarian masses across all cohorts, and improved to AUCs of 0.95–0.99 when combined with risk of ovarian malignancy algorithm (ROMA). Lastly, we validated the metabolic biomarkers in LC-MS and evaluated their effects on OC cell biological behaviours in vitro, including proliferation, colony formation, migration, and apoptosis. Therefore, this study would contribute to the advancement of biomarkers for OC diagnosis with potential clinical translations.

Methods

Chemicals and reagents

The work used reagents for matrix preparation and metabolic analysis. Trisodium citrate dihydrate (catalogue number, (Cat#)10019408), ethylene glycol (Cat#10009818), and ethanol (Cat#10009218) were acquired from Sinopharm Chemical Reagent (Shanghai, China). Sodium acetate anhydrous (Cat#S431678) and ferric chloride hexahydrate (Cat#I431122) were purchased from Aladdin Reagent (Shanghai, China). α-cyano-4-hydroxycinnamic acid (CHCA, Cat#476870), 2,5-dihydroxybenzoic acid (DHB, Cat#85707), glycine (Cat#G7126), valine (Cat#V0500), lysine (Cat#62840), glucose (Cat#G8270), sucrose (Cat#V900116), pyrrole-2-carboxylic acid (PCA, Cat#P73609), and histidine (Cat#53319) were sourced from Sigma-Aldrich (St. Louis, MO, USA). Trifluoroacetic acid (TFA, Cat#T822118) and dihydrothymine (Cat#D873300) were acquired from Macklin Biochemical Co., Ltd. (Shanghai, China). We used all reagents in their as-received condition without further processing. Throughout our experiments, we used deionized water (DIW) with a resistivity of 18.2 MΩ cm in a Milli-Q system (Millipore GmbH, Germany).

Preparation and characterization of nanoparticles

We prepared ferric oxide nanoparticles using a modified solvothermal method reported previously.[35] The preparation involved dissolving 0.6 g of ferric chloride hexahydrate, 0.15 g of trisodium citrate dihydrate, and 0.96 g of anhydrous sodium acetate in 25 mL of ethylene glycol. This solution was then subjected to a solvothermal reaction at 200 °C for 10 h. Finally, the nanoparticles were washed DIW at least 5 times with to remove impurities. We employed various analytical techniques for nanoparticle characterization. Transmission electron microscopy (TEM), along with selected area electron diffraction (SAED) and elemental mapping, was performed using a JEOL JEM-2100F. The nanoparticles were also examined via scanning electron microscopy (SEM) on a Gemini 300 system (ZEISS Ltd., Oberkochen, Germany). The absorption at the wavelength of 355 nm of nanoparticles were measured via ultraviolet–visible (UV–Vis) spectroscopy. Size distribution was evaluated through dynamic light scattering (DLS) on a Mastersizer 2000 instrument. A KEYENCE VK-X3000 was used to determine the co-crystallization of nanoparticles or organic matrices. We captured digital images of the on-chip microarray using a Huawei P40 Pro smartphone.

Ethics

Our research adhered to the ethical guidelines outlined in the Declaration of Helsinki. All participants proved their written informed consent before enrolling in our research. Ethics approval was granted by the Ethics Committee of Renji Hospital, School of Medicine, Shanghai Jiao Tong University (2018-114).

Participant cohort and sample collection

Serum samples of 1691 OC-associated subjects were obtained and this study included 1432 subjects, with 1073 subjects in retrospective cohort and 359 subjects in set-aside validation cohort. The set-aside validation cohort was not used during model development and initial independent verification. The clinical data were collected, including age, body mass index (BMI), glucose, CA-125, HE-4, menopausal status, diabetes history, FIGO stage, and subtype. CA-125 and HE-4 were quantified using electrochemiluminescence immunoassays on a Roche Cobas e801 analyser (Roche Diagnostics, Switzerland). Commercial kits (Roche Elecsys® CA-125 II and HE-4 assays) were employed following manufacturer protocols. Two experienced pathologists independently diagnosed subjects based on pathological examination and were blinded to SMFs analysis. Similarly, researchers performing SMFs analysis were blinded to pathological diagnosis process. We obtained serum samples using standard venous draw procedures from fasted subjects. For OC and benign ovarian disease patients, samples were collected before surgery, while for healthy controls, samples were collected during routine health examinations. Serum isolation was achieved by centrifugation at 2000 g for 10 min. The extracted serum was promptly aliquoted into microtubes and cryopreserved at –80 °C for subsequent analysis. The metabolic database was recorded

using the serum samples that underwent one freeze–thaw cycle. The SMFs data of retrospective cohort was constructed in August 2023, while the SMFs data for set-aside validation cohort was collected in September 2024.

LDI-MS experiments

The LDI-MS experiments were carried out using either Autoflex of TOF-MS or SolariX 7.0T of FT-ICR-MS (Bruker). To prepare organic matrices, 10 mg of CHCA or DHB were dissolved in 1 mL of a 3:7 (v/v) mixture of acetonitrile and 0.1% TFA solution. The nanoparticle powder was dispersed in DIW at a concentration of 1.0 mg/mL. In preparation for LDI-MS analysis, we applied 1.5 μL aliquots of samples (standard metabolite or ten-times diluted serum) onto a 384-well polished steel target. The spotted samples were then left to air-dry completely. Afterward, matrix solution was applied to each spot and dried before MS analysis. In LDI-MS experiments, the pulse frequency was set to 1000 Hz, with 2000 laser shots per analysis. Therefore, we achieved an automatic detection process of ∼15 s per sample, which included ∼2 s for sample detection and ∼1 s interval between samples. This process was repeated for 5 replicates to ensure data reliability.

LC-MS experiments

The LC-MS was used for quantification of glucose, histidine, PCA, and dihydrothymine in serum samples, including sample preparation, chromatographic separation, and MS detection. Sample preparation was initiated by homogenizing 20 μL of serum sample with 60 μL of internal standard solution. Following centrifugation at 14,000 rpm for 5 min, 50 μL of the resultant supernatant was mixed with 50 μL of DIW, yielding a 1:1 diluted sample. For glucose and histidine analysis, a 20 μL aliquot of this 1:1 diluted sample was further diluted with 180 μL of DIW (1:10 dilution). The remaining 80 μL of the 1:1 diluted sample was used directly for PCA and dihydrothymine analysis.

Chromatographic separation was achieved using a Phenomenex PFP column (100 × 3 mm, 2.6 μm). The mobile phase included 0.1% formic acid in water (A) and acetonitrile (B), which maintained a flow rate of 0.5 mL per minute during detection. A gradient elution program was employed, with mobile phase B increasing from 2% to 90% over 4 min before returning to initial conditions. MS detection was performed with a source temperature of 450 °C and an ion spray voltage of 5500 V. Quantification was achieved using multiple reaction monitoring mode with an internal standard method.

Biological function validation

The cell proliferation, colony formation, migration, and apoptosis assays were conducted to verify biological function of metabolic biomarkers, using 2 representative OC cell lines, HEY (RRID: CVCL_0297) and OVCAR-8 (RRID: CVCL_1629). Higher concentrations than physiologically relevant levels of metabolites were selected to ensure detectable biological effects in cellular responses. Similar approaches have been reported in other studies.[36,37] For proliferation assay, HEY cells (3000 cells per well) and OVCAR-8 cells (4000 cells per well) were plated and stayed overnight to ensure cells to adhere to the surface of plate bottom. The cells were subsequently exposed to various concentrations of metabolites for 72 h. During this treatment, the foetal bovine serum (Cat#FSP500, ExCell Bio) concentration was reduced to 2% for HEY cells and 10% for OVCAR-8 cells. Following medium replacement, 10 μL of CCK-8 solution (Cat#PF00004, Proteintech) was introduced and incubated for 1.5 h. The optical density (OD) was measured at a wavelength of 450 nm with a microplate reader (Thermo Fisher Scientific, Shanghai, China). The proliferation rate was calculated as: (OD treated - OD blank)/(OD control - OD blank) × 100%. For colony formation, HEY cells (500 cells per well) and OVCAR-8 cells (1000 cells per well) were plated in 6-well plates and exposed to metabolites. Colonies were fixed with 4% fixation solution for 30 min, followed by a PBS wash and staining with 0.1% crystal violet (Cat#BL802A, Biosharp) for 20 min. The plates were ultimately scanned by a desktop scanner (Epson Co., Ltd., Beijing, China).

To assess cell migration, HEY cells (2.5×10^5 cells per well) and OVCAR-8 cells (5×10^5 cells per well) were plated in 12-well plates. The cell monolayer would be scratched with a 200 μL plastic pipette tip by drawing a straight line across the well centre once cells reached desired confluence. After washing with PBS, a serum-free medium containing various concentrations of metabolites was added. Wound closure was observed every 12 h using an inverted microscope (Echo, San Diego, USA), and the wound area was measured using ImageJ software. Apoptosis assay followed instructions provided by the Annexin V-FITC/PI apoptosis assay kit (#CatBL110A, Biosharp). Cells (1×10^5 per well) were seeded into 6-well plates and exposed to metabolites for 72 h. After treatment, cells were harvested, rinsed with PBS, and resuspended in 250 μL of 1 × binding buffer. 100 μL of resuspension was taken and then stained with 5 μL of Annexin V-FITC for 10 min, followed by addition of 10 μL of PI, before being analysed using a BD FACSCelesta flow cytometer (BD Biosciences, NJ, USA). The resulting data were processed with FlowJo software (version 10.10.0). All experiments were conducted in triplicate.

Data processing

We used Python version 3 for both m/z feature extraction and machine learning implementation. For m/z feature extraction, the m/z features with a S/N ≥3 were extracted using local maximum algorithm in scipy package.[38] Further, peak alignment was performed,

followed by filtration to retain only those m/z features with missing value ratio no more than 1/3 in OC/Non-OC group and the remaining missing value was imputed by local maximum of original spectrum.[39–41] Bruker Compass DataAnalysis software (version 5.0) was used to annotate adduct species and molecular formulae in FT-ICR-MS.[30] For metabolites with multiple adduct forms (e.g., $[M+Na]^+$ and $[M+K]^+$), the sum of all detected adduct intensities was used for quantification to provide a comprehensive measure of metabolite abundance. The identified molecular formulae were cross-referenced with the Human Metabolome Database (HMDB) for putative metabolite identification.[42]

For machine learning, we employed 5 supervised models, including neural network (NN), elastic network (EN), lasso regression (LR), ridge regression (RR), and support vector machine (SVM). These algorithms were implemented via the scikit-learn library.[43] The detailed parameter settings were as follows: For NN, the solver was set to 'adam', the activation function to 'relu', and the regularization term of alpha was optimized to 0.25, with a hidden layer size of (100, 50). For EN, the regularization parameter (C) was set to 1 and the l1_ratio was optimized to 0.2. The regularization parameter (C) for LASSO and RR were optimized to 0.6 and 0.15, respectively. For SVM, the regularization parameter (C) was optimized to 0.02, the kernel was specified as 'linear', and the gamma parameter was set to 'scale'. For threshold optimization of feature selection in LASSO model, a logistic regression model was used with penalty was set to 'none'. The random_state parameter was set to 1 for all models to ensure reproducible results. Receiver operating characteristic (ROC) curves were generated using scikit-learn's roc_curve function with 2000 interpolation points.[43] Confidence intervals for AUCs were calculated using the DeLong's method.[44,45] We used 5-fold cross-validation on the discovery cohort, using 80% of samples for training and 20% for validation in each iteration. This process was repeated 20 iterations with different random splits to ensure robust performance estimation. The independent verification and set-aside validation cohorts were held out during model development and used only for unbiased evaluation of final model's generalizability. For all machine learning performance evaluations, model coefficients were fixed after training in the discovery cohort and applied directly to both the independent verification and set-aside validation cohorts without any retraining, ensuring an unbiased assessment of model's generalization ability. We primarily assessed diagnostic performance using AUC as a threshold-independent measure, while also examining specificity at fixed sensitivity thresholds (0.90, 0.95, and 0.98). The task was considered as a binary classification problem, with each model outputting the probability of a sample being classified as OC.

Statistics

We used Python version 3, specifically employing scikit-learn and umap-learn libraries, to conduct unsupervised analysis of principal component (PC) analysis, t-distributed stochastic neighbour embedding (t-SNE), and uniform manifold approximation and projection (UMAP).[43,46] Statistical power was evaluated using MetaboAnalyst 5.0 with FDR thresholds of 0.10 and 0.05.[47] Microsoft Excel software facilitated the computation of Student's t-test *p*-values. For potential confounding factor analysis, we performed multivariate logistic regression adjusting for age, menopausal status, BMI, and diabetes status. We also conducted stratified analyses to assess the consistency of our findings across different patient subgroups and continuous variables were categorized as follows: age (<50 years and ≥50 years), BMI (<25 kg/m^2 and ≥25 kg/m^2). Subjects with missing values for these factors were excluded from the relevant analyses. For biological function validation, we performed multiple comparisons via Analysis of Variance (ANOVA) using GraphPad Prism 9.5.1 (GraphPad Software Inc., USA). Rstudio 2022.12.0 was employed for Delong test and analysis of similarity (ANOSIM). ANOSIM test was performed using the vegan R package to assess potential batch effects between different NELDI-MS chips.[48] Across all statistical evaluations, ns, *, **, ***, and **** represent $p > 0.05$, $p < 0.05$, $p < 0.01$, $p < 0.001$, and $p < 0.0001$, respectively.

Role of funders

The funders of the study had no role in study design, data collection, data analysis, data interpretation, or writing of this report. The decision to submit this manuscript for publication was made by the listed publication authors with no influence from the funders.

Results

Cohort characteristics and study design

We established an ovarian disease biobank at Renji Hospital, collecting serum samples from 1691 subjects. Of these, 135 with preoperative chemoradiotherapy, 34 with metastatic ovarian tumour, 65 with history of surgery for malignant tumour, and 25 without pathological diagnosis were excluded. Finally, 662 OC and 770 Non-OC subjects (563 benign ovarian disease and 207 healthy control) were enrolled for further analysis, including 1073 subjects (419 OC, 447 benign ovarian disease, and 207 healthy control) in retrospective cohort and 359 subjects (243 OC and 116 benign ovarian disease) in set-aside validation cohort (Fig. 1a). The main purpose of this study was to identify metabolic biomarkers for distinguishing between malignant and benign ovarian masses. While healthy controls were included in the retrospective cohort to help establish baseline metabolic profiles, the set-aside validation cohort was specifically designed to evaluate this

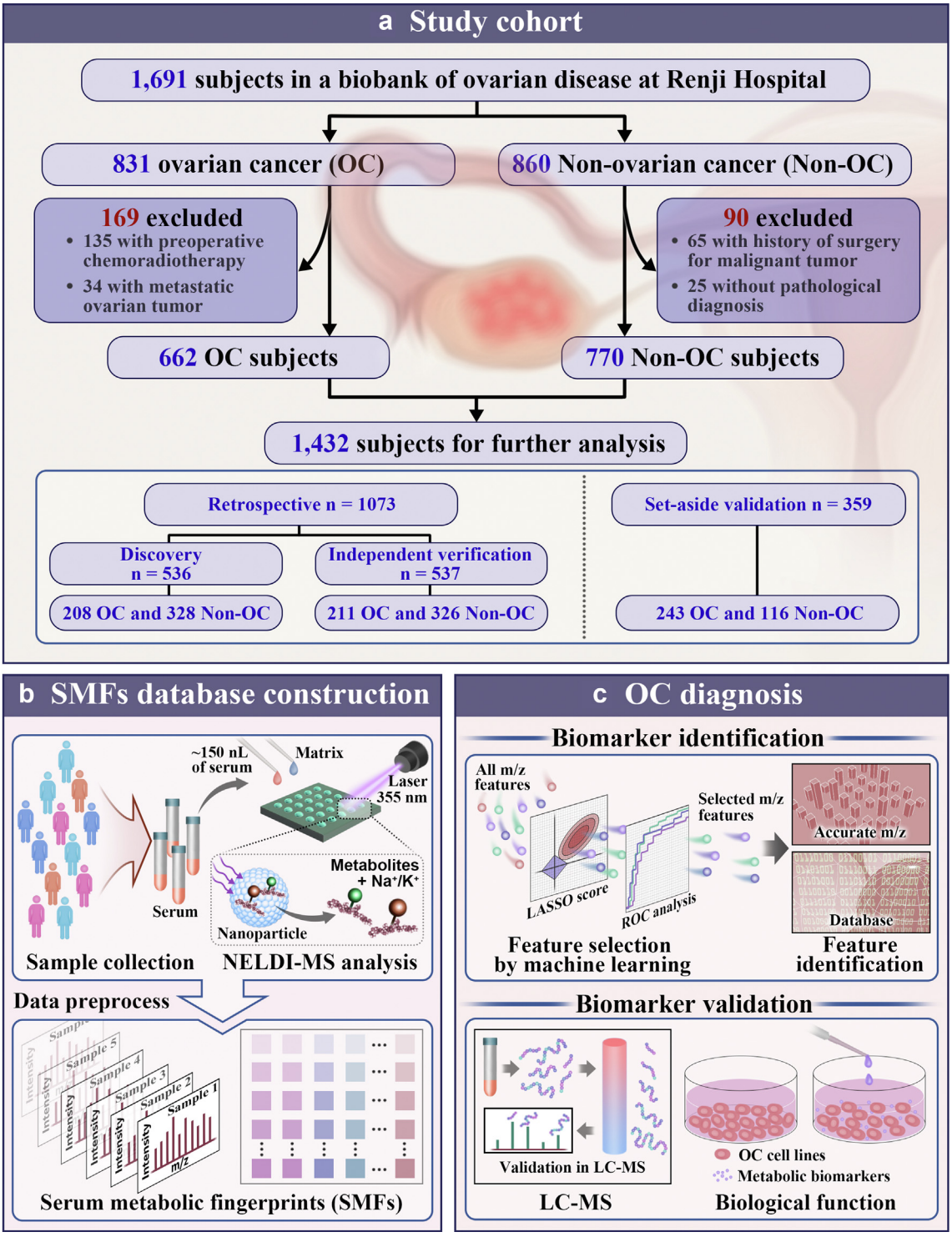

Fig. 1: **Cohort characteristics and study design. a)** 662 OC patients and 770 Non-OC subjects (563 benign ovarian disease patients and 207 healthy controls) were enrolled from 1691 subjects for further analysis, including 1073 subjects (419 OC and 654 Non-OC) in retrospective cohort and 359 subjects (243 OC and 116 Non-OC) in set-aside validation cohort. The retrospective cohort was divided into discovery cohort (208 OC and 328 Non-OC) and independent verification cohort (211 OC and 326 Non-OC). **b)** Construction of serum metabolic fingerprints (SMFs) database using nanoparticle-enhanced laser desorption/ionization mass spectrometry (NELDI-MS) analysis. ~150 nL of serum was analysed with nanoparticle matrix under a 355 nm laser to record raw mass spectra, which were then preprocessed to obtain SMFs. **c)** OC diagnosis workflow, including biomarker identification through accurate m/z search in database based on selected m/z features by machine learning, and biomarker validation using LC-MS and biological functional assays in OC cell lines.

diagnostic capability. The retrospective cohort was divided into discovery cohort (208 OC and 328 Non-OC) and independent verification cohort (211 OC and 326 Non-OC). Clinical characteristics such as age and BMI were collected and summarized in Supplementary Tables S1 and S2. Notably, these data reflected the known epidemiology of OC, which predominantly affects older and postmenopausal women.[49]

Firstly, we used NELDI-MS to construct the OC-associated SMFs database. A 150 nL serum sample was analysed with nanoparticle matrix under a laser of 355 nm (Nd:YAG laser) in NELDI-MS to record raw mass spectra, which were preprocessed to obtain SMFs (Fig. 1b). Then, we identified a metabolic biomarker panel, including glucose, histidine, PCA, and dihydrothymine, through feature selection by machine learning of SMFs and accurate m/z search in database (Fig. 1c). Combining these metabolic biomarkers with ROMA (a risk assessment algorithm combining CA-125, HE-4, and menopausal status) achieved enhanced diagnostic performance for OC. Lastly, we validated the 4 metabolic biomarkers using LC-MS and assessed their effect on OC cell biological behaviours in vitro, including proliferation, colony formation, migration, and apoptosis (Fig. 1c).

Construction of OC-associated SMFs database

Metabolic alterations in cancer patients' blood, resulting from cancer cell metabolic reprogramming, have been extensively reported.[50,51] These findings suggest that blood-based metabolic profiling can serve as a reliable indicator of cancers. We first constructed an OC-associated SMFs database of retrospective cohort using NELDI-MS, demonstrating advantages of fast analytical speed, high throughput, and desirable reproducibility.

For fast analytical speed, NELDI-MS offered an overall experimental time (sample treatment and detection) of ~30 s per sample. Ferric oxide nanoparticles (Fig. 2a and b and Supplementary Fig. S1a–d) were used for NELDI-MS analysis, showing strong photon absorption at the wavelength of 355 nm (Supplementary Fig. S1d), compatible with the Nd:YAG laser used in LDI-MS equipment. The nanoparticles allowed direct detection of metabolites in bio-fluids containing high levels of salts and proteins, minimizing sample treatment time to ~15 s per sample. Furthermore, an automatic detection process of ~15 s per sample was performed on NELDI-MS microarray with 384 samples per chip (Fig. 2c). Consequently, we achieved a fast analytical speed, enabling analysis of 1073 serum samples within 15 h and demonstrating the technique's suitability for large-scale clinical applications.

Besides, NELDI-MS displayed a high throughput in constructing the OC-associated SMFs database. Typical MS of OC and Non-OC serum samples recorded ~130,000 data points with a total ion count of ~2.74×10^7, with strong m/z features obtained in the low m/z range (80–400, Fig. 2d). We extracted 333 m/z features (termed SMFs) through data preprocess and constructed blueprint for the 419 OC and 654 Non-OC subjects (Fig. 2e). We calculated intra-group similarity scores of SMFs to characterize SMFs in the same group (Fig. 2f). Notably, the frequency of similarity scores >0.85 reached 95% for both OC and Non-OC groups, indicating high similarity of SMFs within the same group.

For desirable reproducibility, NELDI-MS offered low coefficients of variation (CVs) in both standard metabolites (CVs = 6.5–9.3% for glycine, valine, lysine, glucose, and sucrose, Supplementary Table S3) and serum samples (CVs <30% for 90.6–94.5% m/z features and medians of CVs = 7.6–10.4%, Fig. 2g). This reproducibility was attributed to the uniform co-crystallization of nanoparticles with an arithmetic mean height of 0.20 μm, compared to commonly used organic matrices (CHCA and DHB, $p < 0.01$) with arithmetic mean heights of 0.63–2.33 μm (Fig. 2h). Importantly, unsupervised analysis, including PC analysis, t-SNE, and UMAP, revealed limited batch effect across different chips for the 1073 serum samples ($p > 0.05$ for ANOSIM test, Fig. 2i and Supplementary Fig. S2a–c), demonstrating high quality and reliability of the SMFs database. The unsupervised analysis of SMFs displayed overlap for OC and Non-OC groups in above data visualizations (Fig. 2j–l), indicating the necessity of introducing supervised machine learning algorithms to decode the SMFs for OC diagnosis.

Machine learning of SMFs for OC diagnosis

We employed machine learning for model building to study the potential of SMFs in differentiating OC and Non-OC groups. The discovery cohort of 536 subjects (208 OC and 328 Non-OC) was used for model optimization using 5-fold cross-validation (Fig. 3a). We have matched age distribution ($p > 0.05$) between OC and Non-OC groups in the discovery cohort to mitigate age bias during training phase and panel development. A power analysis based on a preliminary study involving 12 subjects (6/6, OC/Non-OC) demonstrated predicted powers of 0.91 and 0.86 at FDR thresholds of 0.10 and 0.05 by a sample size of 400 (200 per group), respectively, indicating the statistical confidence of our results (Supplementary Fig. S3a and b and Table S4). The independent verification cohort (211 OC/326 Non-OC) was used to evaluate optimal model's reliability (Fig. 3a).

Specifically, we included 5 supervised machine learning algorithms, including neural network (NN), elastic network (EN), least absolute shrinkage and selection operator regression (LASSO), ridge regression (RR), and support vector machine (SVM), to decode the SMFs for OC diagnosis. We defined the 'score' as the model-predicted probability of a subject being diagnosed with OC, and 'average score' refer to the mean

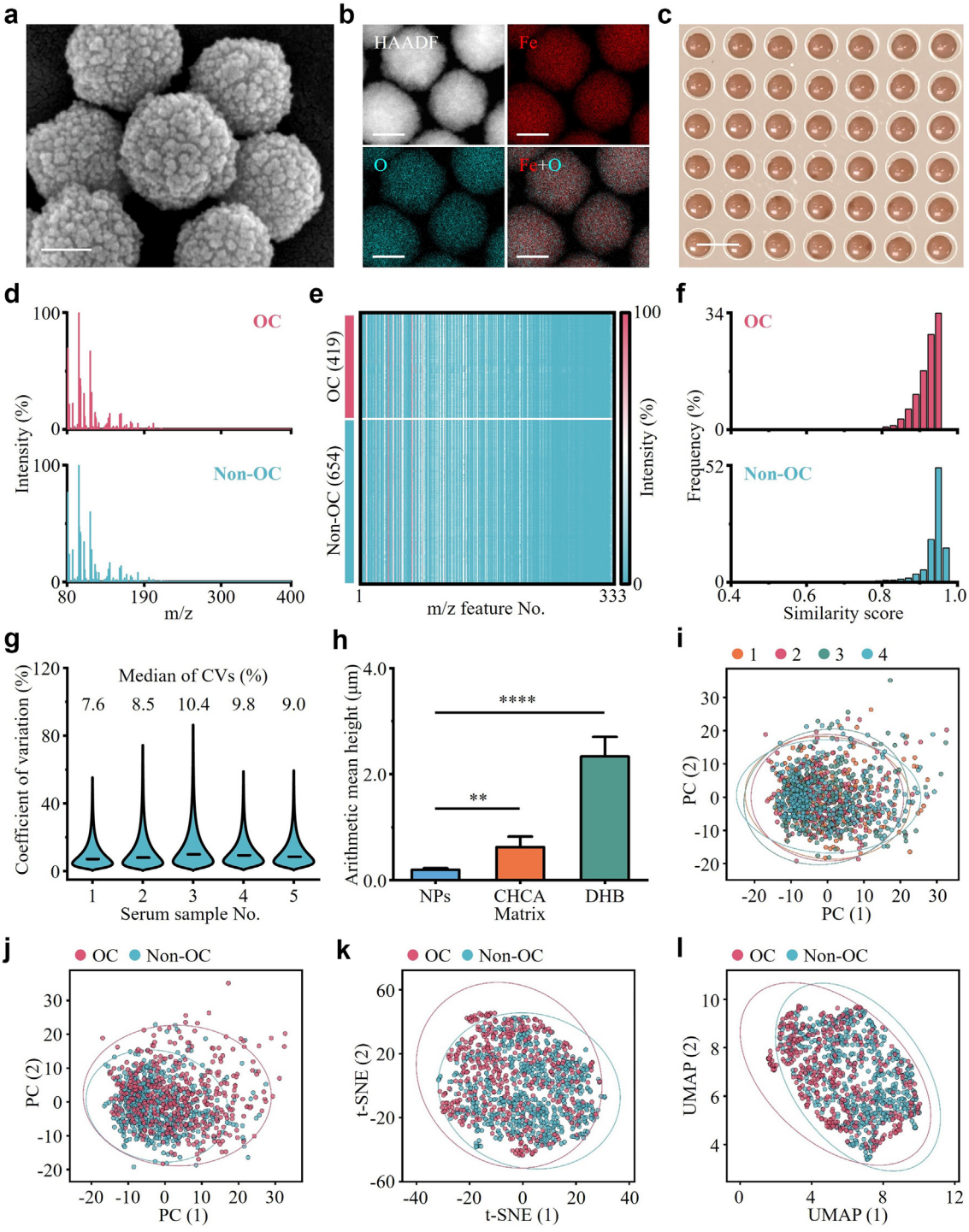

Fig. 2: **Construction of OC-associated SMFs database. a)** Scanning electron microscopy (SEM) image of nanoparticles. Scale bar = 100 nm. **b)** High-angle annular dark-field (HAADF) and elemental mapping of nanoparticles. Scale bar = 100 nm. **c)** Digital image of the NELDI-MS microarray. Scale bar = 5 mm. **d)** Typical mass spectra of serum samples for OC and Non-OC subjects, displaying strong m/z features in the range of 80–400. **e)** Blueprint of OC-associated SMFs for 419 OC and 654 Non-OC subjects was plotted using 333 m/z features. Colour scale was log-corrected. **f)** Frequency distribution of similarity score for OC and Non-OC groups was calculated to characterize SMFs within group. **g)** CV distribution of m/z features was obtained from 5 serum samples in 7 independent replicates, demonstrating high reproducibility (median of CVs = 7.6–10.4%) of NELDI-MS. **h)** Arithmetic mean height of co-crystallization for different matrices (nanoparticles (NPs), α-cyano-4-

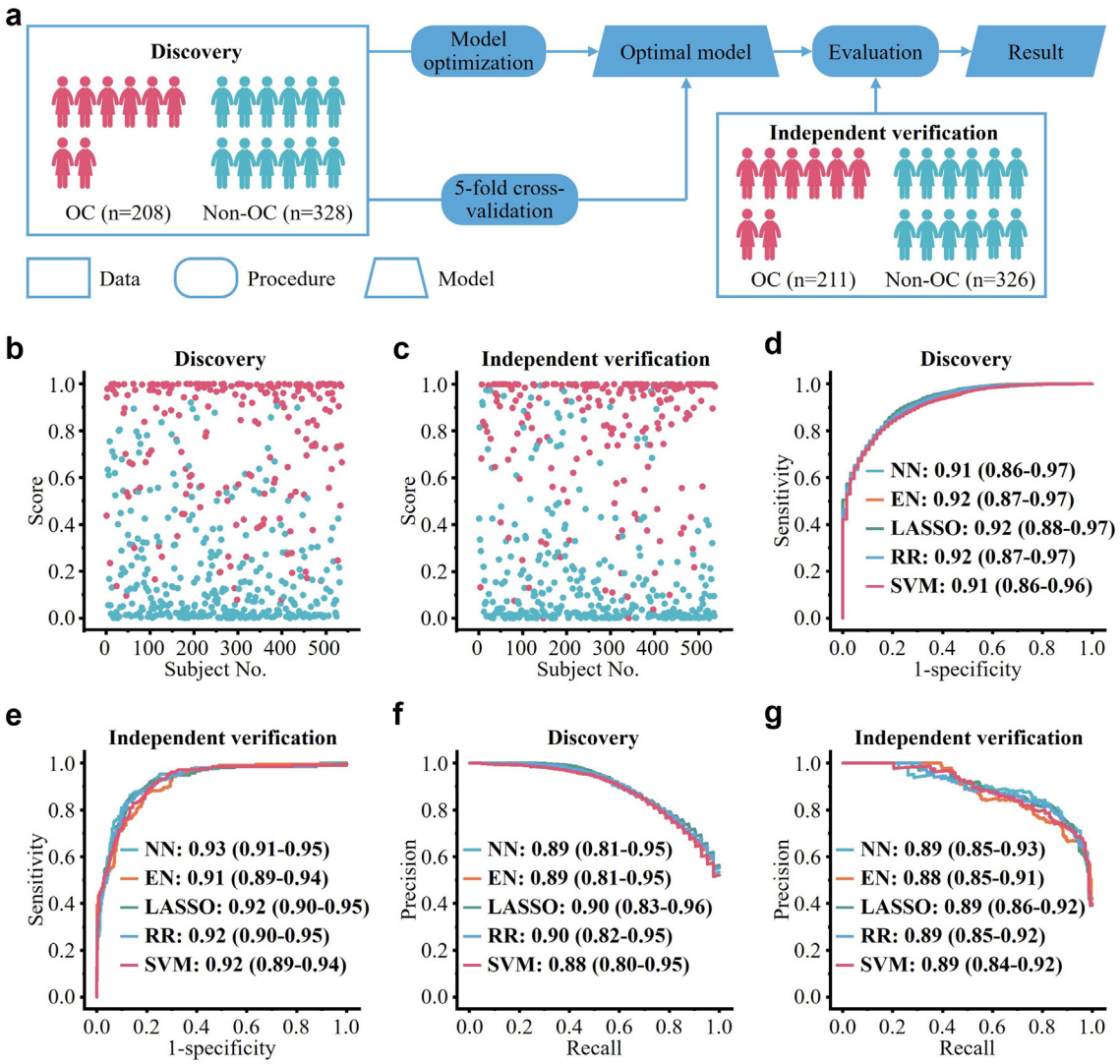

Fig. 3: **Machine learning of SMFs for OC diagnosis. a)** Study design for machine learning of SMFs toward OC diagnosis. The discovery cohort (n = 536, OC/Non-OC = 208/328) was used for model optimization. The optimal model was evaluated in an independent verification cohort (n = 537, OC/Non-OC = 211/326). Scatter plots displayed the scores in LASSO model for both **b)** discovery and **c)** independent verification cohorts. Receiver operating characteristic (ROC) curves of neural network (NN), elastic network (EN), least absolute shrinkage and selection operator regression (LASSO), ridge regression (RR), and support vector machine (SVM) modelled by SMFs with areas under the curve (AUCs) of 0.91–0.92 in **d)** discovery cohort and AUCs of 0.91–0.93 in **e)** independent verification cohort for OC diagnosis. Precision-recall curves (PRCs) of NN, EN, LASSO, RR, and SVM modelled by SMFs with areas under the PRCs (AUPRCs) of 0.88–0.90 in **f)** discovery cohort and AUPRCs of 0.88–0.89 in **g)** independent verification cohort for OC diagnosis.

probability of all subjects within each group. Notably, the scores were significantly higher ($p < 0.001$) in OC group (average scores of 0.698–0.817) compared to Non-OC group (average scores of 0.125–0.254) in both the discovery and independent verification cohorts for all 5 machine learning models (Fig. 3b and c and Supplementary Table S5). These results suggested that alterations in serum metabolic information of OC patients have potential diagnostic value.

hydroxycinnamic acid (CHCA), and 2,5-dihydroxybenzoic acid (DHB)). Error bars represented standard deviation (S.D.) of 5 replicates. **i)** Principal component (PC) analysis of 1073 SMFs with colours annotated by chips, demonstrating limited batch effects ($p > 0.05$ for analysis of similarity) across different chips. **j)** PC analysis, **k)** t-distributed stochastic neighbour embedding (t-SNE), and **l)** uniform manifold approximation and projection (UMAP) showed overlap between OC and Non-OC groups.

The machine learning models based on SMFs demonstrated AUCs of 0.91–0.92 for ROC analysis in the discovery cohort (Fig. 3d). Consistent results (AUCs of 0.91–0.93) were observed in the independent verification cohort (Fig. 3e), showing desirable generalization ability of developed machine learning models. Further, we performed a precision–recall curve (PRC) analysis to validate the diagnostic performance of SMFs-based machine learning models. The areas under PRC were 0.88–0.90 and 0.88–0.89 in the discovery and independent verification cohorts, respectively (Fig. 3f and g). The results of PRC analysis were consistent with ROC analysis and confirmed that the SMFs exhibited desirable performance for OC diagnosis.

Identification and validation of metabolic biomarker panel

To facilitate the practicality of SMFs for OC diagnosis in large-scale clinical settings, we identified a sparse and reliable metabolic biomarker panel through systematic feature selection using only the discovery cohort to avoid potential overfitting. LASSO was chosen as the filtering method due to its L1 regularization that produces sparse solutions, making it particularly suitable for selecting relevant features from high-dimensional metabolomics data.[16,52,53] Starting with all 333 m/z features from the SMFs database, the coefficient threshold of m/z features in LASSO model was optimized to 0.19 based on AUCs in discovery cohort (Fig. 4a and Supplementary Fig. S4), resulting in 35 m/z features. The univariate ROC analysis was then conducted with an AUC threshold of 0.65, yielding 11 m/z features (Fig. 4a), providing an additional filter to ensure selected m/z features possessed sufficient discriminatory power. To ensure biomarker panel reliability, 6 m/z features with mean intensity >500 or paired adducts were included for further identification. Finally, a metabolic biomarker panel consisting of 4 metabolites was obtained through accurate m/z matching (<2 ppm) with HMDB (Supplementary Table S6). Dihydrothymine and glucose were significantly upregulated ($p < 0.01$), while PCA and histidine were downregulated ($p < 0.01$) within OC group, compared to Non-OC group (Fig. 4b). Univariate ROC analysis revealed the limited AUCs of individual metabolic biomarkers ranged from 0.66 to 0.74 in the discovery cohort, 0.55 to 0.76 in the independent verification cohort, and 0.59 to 0.68 in the set-aside validation cohort (Supplementary Table S7).

Clustering analysis of the 4 metabolic biomarkers differentiated ~72% OC and Non-OC subjects, suggesting diagnostic potential of identified biomarker panel (Fig. 4c). Logistic regression of the 4 metabolic biomarkers showed desirable diagnostic performance, with an AUC of 0.88 (95% CI: 0.85–0.91) in the discovery cohort (Fig. 4d) and 0.90 (95% CI: 0.87–0.92) in the independent verification cohort (Fig. 4e). We also evaluated performance of metabolic biomarkers in differentiating the 3 subtypes of OC (serous, endometrioid, and clear cell) from Non-OC, as well as in distinguishing among various OC subtypes. The metabolic biomarkers exhibited consistently high AUCs of 0.88–0.93 for differentiating the 3 subtypes of OC from Non-OC (Supplementary Fig. S5a–c). However, the AUCs for differentiating between OC subtypes were limited, ranging from 0.58 to 0.67 (Supplementary Fig. S5d–f). These results demonstrated the potential of metabolic biomarkers for broad OC diagnosis, while highlighting their limitations in accurately discriminating between OC subtypes.

We randomly selected 70 subjects (35/35, OC/Non-OC, Supplementary Table S8) from retrospective cohort to validate the 4 metabolic biomarkers using LC-MS. The reliability of LC-MS results was confirmed by comparing chromatographic profiles between serum samples and standard metabolites (Supplementary Fig. S6a–d). LC-MS analysis corroborated the up-regulation of dihydrothymine and glucose and the down-regulation of PCA and histidine ($p < 0.05$, Supplementary Fig. S6e), showing consistent performance (AUC of 0.92, 95% CI: 0.86–0.98) for OC diagnosis (Fig. 4f). We have collected metabolic data of retrospective cohort from two different labs using NELDI-MS and observed consistent AUCs (AUC of 0.89, 95% CI: 0.87–0.91 for lab 1 and AUC of 0.90, 95% CI: 0.86–0.93 for lab 2) for OC diagnosis (Fig. 4g). Notably, we further included a set-aside validation cohort (243 OC and 116 benign ovarian disease) to validate the metabolic biomarker panel. To our excitement, SMFs data in the set-aside validation cohort demonstrated consistent results with our retrospective cohort, showing the up-regulation of dihydrothymine and glucose and the down-regulation of PCA and histidine ($p < 0.05$, Fig. 4h). Consequently, the metabolic biomarker panel distinguished OC from benign ovarian disease with an AUC of 0.89 (95% CI: 0.85–0.92) in this set-aside validation cohort (Fig. 4i). To assess the robustness of our metabolic biomarker panel in its intended clinical setting - distinguishing between malignant and benign ovarian masses, we performed additional analyses excluding healthy controls. The panel maintained strong diagnostic performance with AUCs of 0.87 (95% CI: 0.83–0.90), 0.88 (95% CI: 0.85–0.92), and 0.89 (95% CI: 0.86–0.92) in the discovery, independent verification, and set-aside validation cohorts, respectively (Supplementary Fig. S7a–c). These results demonstrated reproducibility of our results between different instruments, labs, and cohorts.

Performance comparison with existing diagnostic biomarkers

We compared the diagnostic performance of metabolic biomarkers with existing biomarkers of CA-125, HE-4, and ROMA in both the discovery and independent verification cohorts. Further, we evaluated the potential

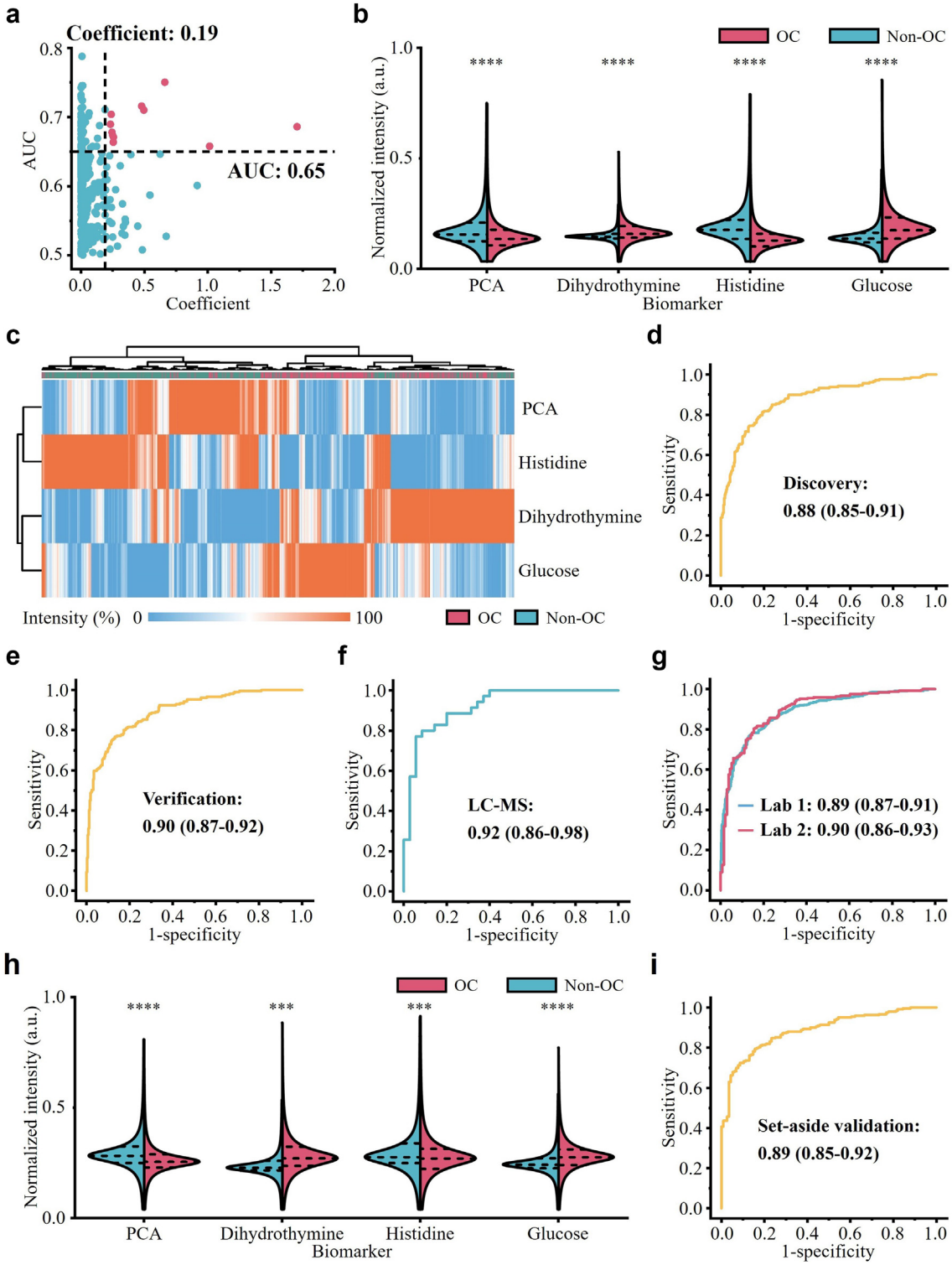

Fig. 4: **Identification and validation of metabolic biomarker panel. a)** The m/z features were selected from SMFs using the criteria of coefficient ≥0.19 in LASSO model and AUC ≥0.65. **b)** Violin plot showed differential expression of metabolic biomarkers between OC and Non-OC groups in NELDI-MS. **c)** Clustering analysis of 4 metabolic biomarkers differentiated ~72% OC and Non-OC subjects, suggesting diagnostic potential of the identified biomarker panel. ROC curves of the metabolic biomarker panel showed an AUC of 0.88 (95% CI:

of combining ROMA with metabolic biomarkers to enhance diagnostic performance. These analyses included only OC and benign ovarian disease patients, considering that ROMA is specifically designed for differentiating malignant from benign ovarian masses. In the discovery cohort, metabolic biomarker panel demonstrated an AUC of 0.89 (95% CI: 0.84–0.94), comparable to ROMA (AUC = 0.88, 95% CI: 0.82–0.93), higher than CA-125 (AUC = 0.86, 95% CI: 0.80–0.92) and HE-4 (AUC = 0.85, 95% CI: 0.78–0.91) for OC diagnosis (Fig. 5a). Similar results were observed in early-stage OC (Fig. 5b) and independent verification cohort (Supplementary Fig. S8a and b).

We further combined metabolic biomarker panel with ROMA using logistic regression and observed that both metabolic biomarker panel and ROMA were statistically significant predictors ($p < 0.01$) for OC diagnosis. Notably, combined analysis showed a higher ($p < 0.05$) average diagnostic score of 0.93 in advanced-stage OC subjects, compared with early-stage OC (average score of 0.87) and benign ovarian disease (average score of 0.16) subjects (Fig. 5c). The combined analysis improved ($p < 0.05$) AUCs to 0.96 (95% CI: 0.93–0.99) and 0.98 (95% CI: 0.96–1.00) for discovery (Fig. 5a) and independent verification (Supplementary Fig. S8a) cohorts, respectively. Similar results were observed in early-stage OC (Fig. 5b and Supplementary Fig. S8b). Besides, the combined analysis showed an improved specificity ($p < 0.05$) of 59.1–87.9%, vs. 18.2–66.7% for metabolic biomarkers, 0.0–54.5% for ROMA, 0.0–39.4% for HE-4, and 6.1–43.9% for CA-125 with sensitivities of 90%, 95%, and 98% (Fig. 5d). The enhancement of specificity was also observed in early-stage OC (Fig. 5e, $p < 0.05$) and independent verification cohort (Supplementary Fig. S9a and b, $p < 0.05$). These results highlight the diagnostic benefits of integrating metabolic profiling with ROMA.

To assess whether clinical factors of age and menopausal status influenced our metabolic biomarker panel's performance, we conducted stratified and adjusted analyses in the discovery cohort. The panel maintained consistent AUCs across different subgroups (Fig. 5f–h): pre-menopausal (AUC = 0.86, 95% CI: 0.82–0.91), post-menopausal (AUC = 0.88, 95% CI: 0.83–0.93), age <50 (AUC = 0.85, 95% CI: 0.80–0.90), age ≥50 (AUC = 0.89, 95% CI: 0.85–0.93), BMI <25 (AUC = 0.88, 95% CI: 0.83–0.93), and BMI ≥25 (AUC = 0.85, 95% CI: 0.73–0.96). In multivariate models adjusting for age and menopausal status (Supplementary Table S9), all metabolic biomarkers remained significant predictors ($p < 0.01$) of OC, indicating their diagnostic value independent of clinical factors. We further investigated whether diabetes might influence our metabolic biomarker panel's performance. Analysis revealed that glucose levels remained significantly higher in OC patients compared to Non-OC subjects, even in the non-diabetic subpopulation (retrospective: 5.14 mM vs. 4.84 mM, $p < 0.001$; set-aside validation: 5.08 mM vs. 4.45 mM, $p < 0.001$). Our model maintained robust performance in non-diabetic subjects with AUCs of 0.86–0.92 across all cohorts (Supplementary Fig. S10a-c). Multivariate analysis confirmed that diabetes was not a significant predictor ($p = 0.28$) when included alongside our metabolic biomarkers (Supplementary Table S10), demonstrating that our panel's diagnostic capability for OC is independent of diabetes status.

Biological function validation of metabolic biomarkers

We employed 2 representative OC cell lines, HEY and OVCAR-8, to assess biological function of metabolites, concerning cell proliferation, colony formation, migration, and apoptosis. HEY and OVCAR-8 cell lines were selected as they represent well-characterized models of high-grade serous OC, the most common subtype accounting for ~70% of OC cases.[50] Firstly, we evaluated glucose, histidine, PCA, and dihydrothymine on OC cell proliferation and colony formation. Glucose significantly promoted ($p < 0.05$) cell proliferation at concentrations of 5–20 mM in both HEY and OVCAR-8 cell lines, while histidine and PCA exhibited concentration-dependent inhibitory effects ($p < 0.05$, Fig. 6a). Dihydrothymine, however, showed no significant effect ($p > 0.05$) at concentrations ranging from 30 μM to 1000 μM in either cell line (Fig. 6a). These findings were corroborated by observations from colony formation assays (Fig. 6b).

Subsequently, we performed wound healing assays to evaluate cellular migration (Fig. 6c). Glucose significantly accelerated ($p < 0.05$) wound closure in OVCAR-8 cells at concentrations ranging from 5 mM to 20 mM, whereas PCA exhibited inhibitory effects ($p < 0.05$) at both 4 mM and 8 mM. Histidine impeded ($p < 0.05$) wound healing process in both HEY and OVCAR-8 cells at concentration of 30 mM. In contrast, dihydrothymine had no significant effect ($p > 0.05$) on wound closure in either cell line. Finally, we used flow cytometric analysis

0.85–0.91) in the **d)** discovery cohort and 0.90 (95% CI: 0.87–0.92) in the **e)** independent verification cohort for OC diagnosis. **f)** ROC curve of the metabolic biomarker panel showed an AUC of 0.92 (95% CI: 0.86–0.98) for OC diagnosis using LC-MS. **g)** ROC curves of the metabolic biomarker panel showed consistent performance (AUC of 0.89, 95% CI: 0.87–0.91 for lab 1 and AUC of 0.90, 95% CI: 0.86–0.93 for lab 2) for OC diagnosis using NELDI-MS. **h)** Violin plot showed differential expression of metabolic biomarkers between OC and benign ovarian disease groups in set-aside validation cohort. **i)** ROC curve of the metabolic biomarker panel showed AUC of 0.89 (95% CI: 0.85–0.92) in set-aside validation cohort for OC diagnosis.

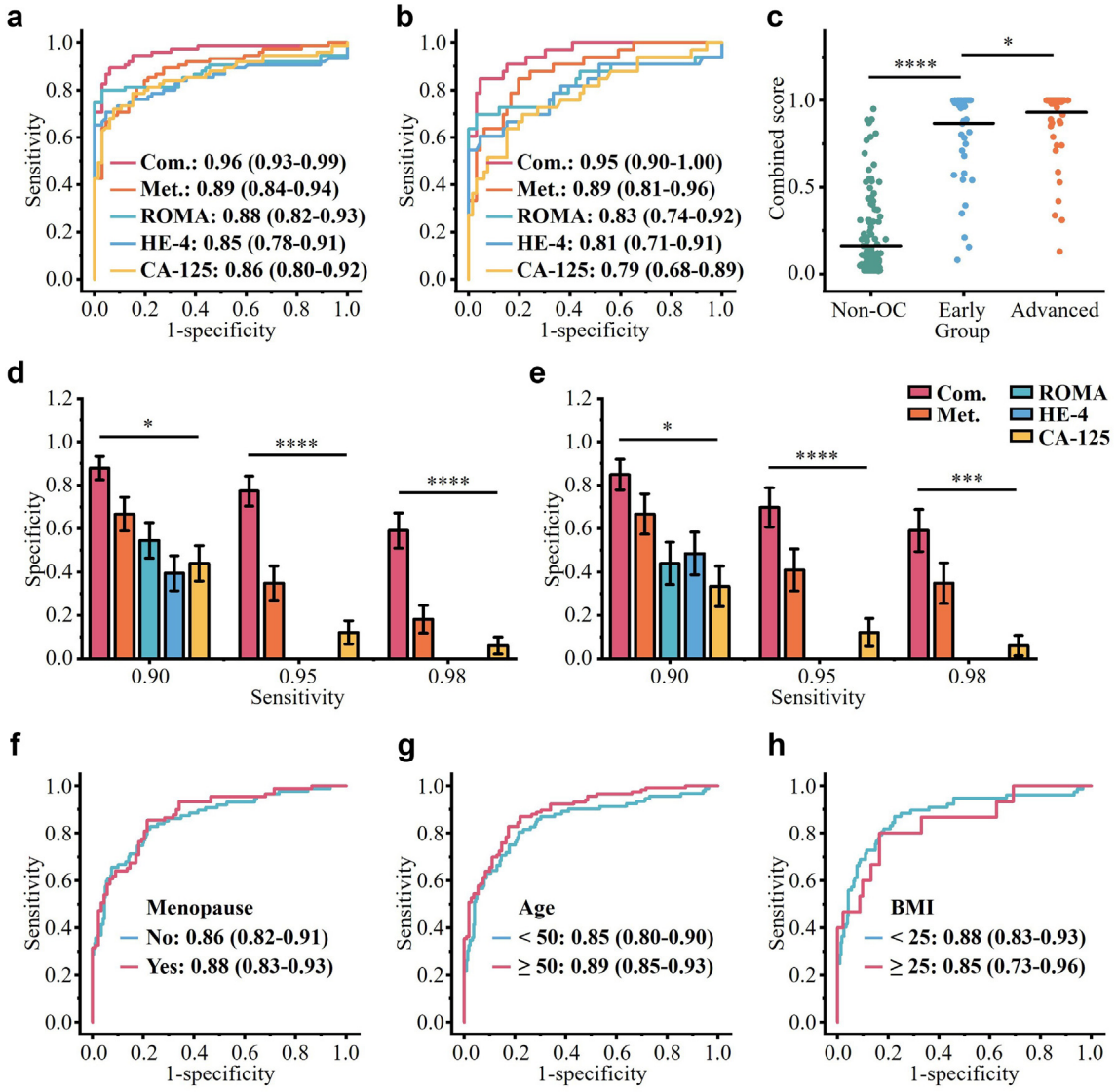

Fig. 5: **Performance comparison with existing diagnostic biomarkers.** ROC curves of combined analysis (Com.), metabolic biomarkers (Met.), ROMA, HE-4, and CA-125 for **a)** OC diagnosis and **b)** early-stage OC diagnosis in the discovery cohort. **c)** Score distribution of subjects from Non-OC (benign ovarian disease) and OC group (early and advanced stages) for combined analysis. Specificities for combined analysis (Com.), metabolic biomarkers (Met.), ROMA, HE-4, and CA-125 at sensitivities of 90.0%, 95.0%, and 98.0% for **d)** OC diagnosis and **e)** early-stage OC diagnosis in the discovery cohort. ROC curves of the metabolic biomarker panel stratified by **f)** menopausal status: pre-menopausal (AUC = 0.86, 95% CI: 0.82–0.91) and post-menopausal (AUC = 0.88, 95% CI: 0.83–0.93), **g)** age: <50 years (AUC = 0.85, 95% CI: 0.80–0.90) and ≥50 years (AUC = 0.89, 95% CI: 0.85–0.93), and **h)** BMI: <25 kg/m^2 (AUC = 0.88, 95% CI: 0.83–0.93) and ≥25 kg/m^2 (AUC = 0.85, 95% CI: 0.73–0.96).

to assess the effects of these metabolites on cell apoptosis (Supplementary Fig. S11). Glucose significantly suppressed apoptosis, while histidine and PCA induced apoptotic responses in both cell lines ($p < 0.05$). Dihydrothymine showed no significant effect ($p > 0.05$) on apoptosis rate at concentrations up to 1000 μM. In summary, these in vitro observations provide initial biological context for the metabolic alterations observed in our diagnostic panel, though further investigation would be needed to fully understand their roles in OC development.

Discussion

Our machine learning model aims to diagnose OC by analysing metabolites in blood samples, developed using data from over 1400 subjects. We tested 5 machine learning algorithms using 5-fold cross-validation on discovery cohort and validated on independent

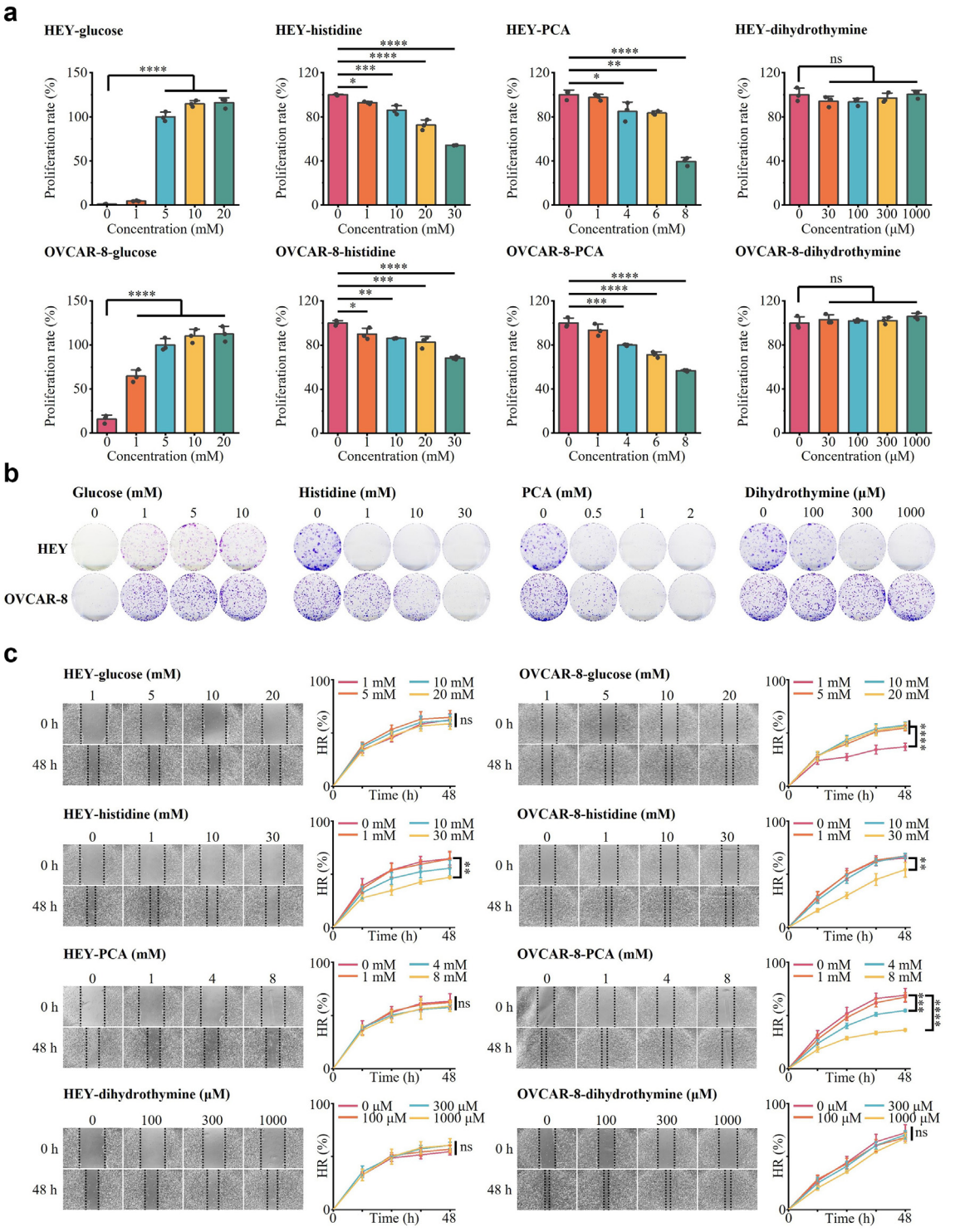

Fig. 6: **Biological function validation of metabolic biomarkers. a)** Proliferation rate of HEY and OVCAR-8 cells treated with varying concentrations of glucose, histidine, PCA, and dihydrothymine. **b)** Colony formation assay of HEY and OVCAR-8 cells treated with different concentrations of glucose, histidine, PCA, and dihydrothymine. **c)** Wound healing assay showed migration of HEY and OVCAR-8 cells treated with various concentrations of glucose, histidine, PCA, and dihydrothymine. Images were captured at 0 and 48 h with corresponding quantification of healing rate (HR). Error bars represented S.D. of 3 independent experiments.

verification cohort (Fig. 3a). We identified and validated 4 key metabolic biomarkers (glucose, histidine, PCA, and dihydrothymine), achieving AUCs of 0.87–0.89 for distinguishing between malignant and benign ovarian masses. When combined with existing clinical tests (ROMA), performance improves to AUCs of 0.95–0.99. Our approach offers advantages in analytical speed (~30 s/sample) and cost (~2–3 dollars/sample), making it suitable for large-scale screening. The model performs consistently across different patient subgroups regardless of age, menopausal status, BMI, and diabetes status. Future steps include external validation across multiple centres and engineering refinements for clinical adaptation. We envision this test complementing existing approaches to improve early OC detection.

OC ranks the most lethal gynaecological malignancy, accounting for ~200,000 deaths annually, underscoring the urgent need for early diagnosis toward better outcomes.[5,54,55] Given the heterogeneity of epithelial OCs, Type I tumours are generally indolent with precursor lesions, whereas Type II tumours, including high-grade serous OC, are aggressive with early metastatic potential, highlighting the necessity for efficient diagnostic strategies.[56] Transvaginal ultrasound, typically used as initial evaluation for OC, relies on experienced clinicians but offers limited performance (sensitivity/specificity of ~55–85%).[6,7] While biopsy is the gold standard for OC diagnosis, it is invasive with risks (e.g., bleeding and infection) and may result in the spillage of malignant cells into peritoneal cavity. The existing blood biomarkers like CA-125 and HE-4 are limited by suboptimal sensitivity/specificity (~50–70%), particularly for early-stage OC (~50–60%).[7,9–12] Furthermore, multivariate index assays like ROMA enhances diagnostic accuracy for OC. However, its performance remains suboptimal, limiting its widespread clinical application.[57] Consequently, it is urgent to explore alternative biomarkers in blood for early, large-scale diagnosis of OC in clinical settings.

Various biomarkers in blood are studied for OC diagnosis, in terms of genes, proteins, and metabolites.[8,58] For example, BRCA1/2 germline mutations represent the risk factors for epithelial OC, occurring in 6–15% of diagnosed cases.[59] miRNAs have emerged as promising biomarkers for OC detection, but challenges related to sample processing and detection standardization must be overcome.[57] Metabolic biomarkers are particularly promising as they provide a more immediate reflection of disease phenotype.[33] Importantly, metabolic alterations in cancer patients' blood, resulting from cancer cell metabolic reprogramming, can be explored for diagnostics.[20,51] Several metabolomics studies over the past decade have established the foundation for blood-based OC detection.[21,22,60–64] For example, Irajizad et al. identified a 7-marker metabolic panel that achieved an AUC of 0.86 for OC diagnosis and further enhanced specificity when combined with ROMA.[21] Buas et al. found that certain plasma lipids like PS(O-18:0/0:0) and DAG (16:1/18:1) can differentiate OC from benign tumours, and that combining these lipid biomarkers with CA-125 further enhances diagnostic performance.[62,64] However, current studies on blood-based metabolic biomarkers for OC diagnosis are limited by relatively small-scale cohorts (sample sizes of ~200–500), traditional analytical techniques, and a lack of biological functional assays.[10,21–24] In contrast, our study identified a metabolic biomarker panel in blood via a large-scale cohort and advanced analytical techniques, with validation in LC-MS and in vitro biological functional assays, achieving AUCs of 0.87–0.89 and improved to 0.95–0.99 when combined with ROMA for distinguishing between malignant and benign ovarian masses.

Cohort design plays a crucial role in developing metabolic biomarker panels, offering precise insights into disease characteristics. Our study stands out as the largest cohort to date for serum metabolic analysis towards OC diagnosis, significantly surpassing previous studies with relatively small-scale cohorts of ~200–500 subjects.[10,21–24] We enrolled 1432 OC-associated subjects from an ovarian disease biobank at Renji Hospital, applying well-defined criteria. This large-scale cohort significantly enhances the statistical robustness and generalizability of our findings, addressing critical gaps in previous research. Power analyses conducted at FDR thresholds of 0.10 and 0.05 demonstrated predicted powers of 0.91 and 0.86 by a sample size of 400 (200 per group), respectively, which exceeds the threshold of 0.80 for statistical reliability.[65,66]

Regarding analytical techniques, NELDI-MS demonstrated advantages as regards analytical speed and test cost. For analytical speed, the tailored nanoparticles in NELDI-MS allowed direct detection of metabolites in bio-fluids with ~30 s per sample. In contrast, LC/GC-MS requires deproteinization and chromatography in sample preparation to purify and enrich metabolites, resulting in a longer analytical time of ~15–30 min per sample.[30,67] For test cost, the estimated cost for NELDI-MS was ~2–3 dollars per sample, taking into account of all chemical reagents (e.g., nanoparticle synthesis) and equipment maintenance (e.g., Nd:YAG laser).[68,69] In comparison, the costs for LC/GC MS are usually ~tens of dollars, with additional reagents and instruments for deproteinization and chromatography in sample treatment.[70] Further, the costs of screening methods used in clinical settings like ROMA and ultrasound are ~50–150 of dollars.[71,72] Therefore, the analytical speed and test cost make NELDI-MS an attractive option for potential large-scale testing in clinical environments.

Furthermore, our in vitro studies provided initial biological context for the altered metabolite levels observed in OC patients. Consistent with previous research, we observed changes in glucose metabolism, which has been widely studied in cancer cells.[73,74] The

alterations we observed in histidine levels are also intriguing given previous reports about its potential role in cancer treatment.[75,76] While PCA has been less studied in cancer, our preliminary in vitro observations suggest it may influence certain aspects of OC cell behaviour. These in vitro findings provided initial evidence for potential associations between the identified metabolites and OC development. However, the underlying mechanisms leading to serum metabolic alterations in OC patients are complex and warrant further investigation using more sophisticated models such as organoids and animals to fully understand the origin and significance of these metabolic signatures.

In summary, we have constructed a large-scale OC-associated SMFs database comprising 1073 subjects in retrospective cohort and 359 subjects in set-aside validation cohort using NELDI-MS. Then, we identified a biomarker panel of 4 metabolites through machine learning of SMFs, achieving AUCs of 0.95–0.99 when combined with ROMA. Lastly, we validated the metabolic biomarkers in LC-MS and evaluated their effects on OC cell biological behaviours in vitro. Therefore, this study would contribute to the advancement of biomarkers for OC diagnosis with potential clinical translations. However, several limitations should be acknowledged: 1) mass spectrometer and nanoparticles were crucial for metabolic profiling and further engineering of mass spectrometer may be required to adapt this technique for point-of-care testing. 2) While our set-aside validation demonstrates the robustness of our findings, future external validation across multiple independent centres will be valuable to further establish the generalizability of our metabolic biomarker panel. 3) Additional functional validation of the metabolic biomarkers is needed using more sophisticated models such as organoids and animals to fully understand their roles in OC pathogenesis and progression.

Contributors

Conceptualization: WSL, XXH, ZZB, WD, HWL, XY, KQ; Methodology: WSL, YYL, JXZ, SZY, QS; Investigation: WSL, XXH, JXZ, YDH, RMW, XY; Visualization: WSL, XXH, ZZB, YYL, JW, XYX, KQ; Funding acquisition: SZY, YDH, WD, HWL, XY, KQ; Project administration: HWL, XY, KQ; Supervision: WD, HWL, XY, KQ; Writing-original draft: WSL, XXH, ZZB, KQ; Writing-review & editing: WSL, XXH, ZZB, WD, HWL, XY, KQ.

Data sharing statement

The data and supporting analytical code that support the findings of this study can be obtained from the corresponding author upon a reasonable request. The SMFs data have been deposited to the NIH Common Fund's National Metabolomics Data Repository, the Metabolomics Workbench (https://www.metabolomicsworkbench.org) with identifier of ST003815.[77]

Declaration of interests

The authors declare the following competing interests. The authors have filed patents using the methods and technologies to analyse metabolites.

Acknowledgements

The authors gratefully acknowledge financial support from Project 2021YFA0910100 by MOST, Projects 82421001, 823B2050, 824B2059, and 82173077 by NSFC, Medical-Engineering Joint Funds of Shanghai Jiao Tong University (YG2021GD02, YG2024ZD07, and YG2023ZD08), Project 23JC1403000 by Shanghai Science and Technology Committee Project, and Project 2021-01-07-00-02-E00083 by Shanghai Institutions of Higher Learning. This work was also sponsored by the Project 2022XYJG0001-01-16 by Shanghai Jiao Tong University Inner Mongolia Research Institute, Project 2024YFHZ0176 by Sichuan Provincial Department of Science and Technology, Innovation Research Plan by the Shanghai Municipal Education Commission (ZXWF082101), Innovative Research Team of High-Level Local Universities in Shanghai (SHSMU-ZDCX20210700), Basic-Clinical Collaborative Innovation Project from Shanghai Immune Therapy Institute, Guangdong Basic and Applied Basic Research Foundation (2024A1515013255). We thank all the participants for donating their bio-samples and clinical information to this study.

Appendix A. Supplementary data

Supplementary data related to this article can be found at https://doi.org/10.1016/j.ebiom.2025.105706.

References

1 Sung H, Ferlay J, Siegel RL, et al. Global cancer statistics 2020: GLOBOCAN estimates of incidence and mortality worldwide for 36 cancers in 185 countries. *CA Cancer J Clin*. 2021;71(3):209–249.
2 Wang P, Ma J, Li W, et al. Profiling the metabolome of uterine fluid for early detection of ovarian cancer. *Cell Rep Med*. 2023;4(6):101061.
3 Saani I, Raj N, Sood R, et al. Clinical challenges in the management of malignant ovarian germ cell tumours. *Int J Environ Res Public Health*. 2023;20(12):6089.
4 Kim M, Chen C, Wang P, et al. Detection of ovarian cancer via the spectral fingerprinting of quantum-defect-modified carbon nanotubes in serum by machine learning. *Nat Biomed Eng*. 2022;6(3):267–275.
5 Siegel RL, Miller KD, Fuchs HE, Jemal A. Cancer statistics, 2021. *CA Cancer J Clin*. 2021;71(1):7–33.
6 Zhu JW, Charkhchi P, Akbari MR. Potential clinical utility of liquid biopsies in ovarian cancer. *Mol Cancer*. 2022;21(1):114.
7 Gentry-Maharaj A, Burnell M, Dilley J, et al. Serum HE4 and diagnosis of ovarian cancer in postmenopausal women with adnexal masses. *Am J Obstet Gynecol*. 2020;222(1):56.e01–56.e17.
8 Xiao Y, Bi M, Guo H, Li M. Multi-omics approaches for biomarker discovery in early ovarian cancer diagnosis. *EBioMedicine*. 2022;79:104001.
9 Basu P, Vale D. Screening for epithelial ovarian cancer: an updated review. *Indian J Gynecol Oncol*. 2017;15(1):9.
10 Pei C, Wang Y, Ding Y, et al. Designed concave octahedron heterostructures decode distinct metabolic patterns of epithelial ovarian tumors. *Adv Mater*. 2023;35(18):e2209083.
11 Landolfo C, Ceusters J, Valentin L, et al. Comparison of the ADNEX and ROMA risk prediction models for the diagnosis of ovarian cancer: a multicentre external validation in patients who underwent surgery. *Br J Cancer*. 2024;130(6):934–940.
12 Cai G, Huang F, Gao Y, et al. Artificial intelligence-based models enabling accurate diagnosis of ovarian cancer using laboratory tests in China: a multicentre, retrospective cohort study. *Lancet Digit Health*. 2024;6(3):e176–e186.
13 Coscia F, Lengyel E, Duraiswamy J, et al. Multi-level proteomics identifies CT45 as a chemosensitivity mediator and immunotherapy target in ovarian cancer. *Cell*. 2018;175(1):159–170.
14 Ghose A, Bolina A, Mahajan I, et al. Hereditary ovarian cancer: towards a cost-effective prevention strategy. *Int J Environ Res Public Health*. 2022;19(19):12057.
15 El-Deiry WS, Goldberg RM, Lenz HJ, et al. The current state of molecular testing in the treatment of patients with solid tumors, 2019. *CA Cancer J Clin*. 2019;69(4):305–343.
16 Yao Y, Wang X, Guan J, et al. Metabolomic differentiation of benign vs malignant pulmonary nodules with high specificity via high-resolution mass spectrometry analysis of patient sera. *Nat Commun*. 2023;14(1):2339.
17 Ghose A, Gullapalli SVN, Chohan N, et al. Applications of proteomics in ovarian cancer: dawn of a new era. *Proteomes*. 2022;10(2):16.
18 Gong TT, Guo S, Liu FH, et al. Proteomic characterization of epithelial ovarian cancer delineates molecular signatures and

therapeutic targets in distinct histological subtypes. *Nat Commun*. 2023;14(1):7802.
19 Buergel T, Steinfeldt J, Ruyoga G, et al. Metabolomic profiles predict individual multidisease outcomes. *Nat Med*. 2022;28(11):2309–2320.
20 Faubert B, Solmonson A, DeBerardinis RJ. Metabolic reprogramming and cancer progression. *Science*. 2020;368(6487):eaaw5473.
21 Irajizad E, Han CY, Celestino J, et al. A blood-based metabolite panel for distinguishing ovarian cancer from benign pelvic masses. *Clin Cancer Res*. 2022;28(21):4669–4676.
22 Zeleznik OA, Eliassen AH, Kraft P, et al. A prospective analysis of circulating plasma metabolites associated with ovarian cancer risk. *Cancer Res*. 2020;80(6):1357–1367.
23 Ke C, Hou Y, Zhang H, et al. Large-scale profiling of metabolic dysregulation in ovarian cancer. *Int J Cancer*. 2015;136(3):516–526.
24 Garcia E, Andrews C, Hua J, et al. Diagnosis of early stage ovarian cancer by 1H NMR metabonomics of serum explored by use of a microflow NMR probe. *J Proteome Res*. 2011;10(4):1765–1771.
25 Turkoglu O, Zeb A, Graham S, et al. Metabolomics of biomarker discovery in ovarian cancer: a systematic review of the current literature. *Metabolomics*. 2016;12(4):60.
26 Aron AT, Petras D, Schmid R, et al. Native mass spectrometry-based metabolomics identifies metal-binding compounds. *Nat Chem*. 2022;14(1):100–109.
27 De Spiegeleer M, Plekhova V, Geltmeyer J, et al. Point-of-care applicable metabotyping using biofluid-specific electrospun MetaSAMPs directly amenable to ambient LA-REIMS. *Sci Adv*. 2023;9(23):eade9933.
28 Dunn WB, Broadhurst D, Begley P, et al. Procedures for large-scale metabolic profiling of serum and plasma using gas chromatography and liquid chromatography coupled to mass spectrometry. *Nat Protoc*. 2011;6(7):1060–1083.
29 Perez de Souza L, Alseekh S, Scossa F, Fernie AR. Ultra-high-performance liquid chromatography high-resolution mass spectrometry variants for metabolomics research. *Nat Methods*. 2021;18(7):733–746.
30 Sun S, Liu W, Yang J, Wang H, Qian K. Nanoparticle-assisted cation adduction and fragmentation of small metabolites. *Angew Chem Int Ed*. 2021;60(20):11310–11317.
31 Huang Y, Du S, Liu J, et al. Diagnosis and prognosis of breast cancer by high-performance serum metabolic fingerprints. *Proc Natl Acad Sci USA*. 2022;119(12):e2122245119.
32 Chen Y, Xu W, Zhang W, et al. Plasma metabolic fingerprints for large-scale screening and personalized risk stratification of metabolic syndrome. *Cell Rep Med*. 2023;4(7):101109.
33 Xu Z, Huang Y, Hu C, et al. Efficient plasma metabolic fingerprinting as a novel tool for diagnosis and prognosis of gastric cancer: a large-scale, multicentre study. *Gut*. 2023;72(11):2051–2067.
34 Wang R, Gu Z, Wang Y, et al. A "one-stop shop" decision tree for diagnosing and phenotyping polycystic ovarian syndrome on serum metabolic fingerprints. *Adv Funct Mater*. 2022;32(45):2206670.
35 Liu W, Ma J, Zhang J, et al. Identification and validation of serum metabolite biomarkers for endometrial cancer diagnosis. *EMBO Mol Med*. 2024;16(4):988–1003.
36 Yan R, Zhang P, Shen S, et al. Carnosine regulation of intracellular pH homeostasis promotes lysosome-dependent tumor immunoevasion. *Nat Immunol*. 2024;25(3):483–495.
37 Liu J, Geng W, Sun H, et al. Integrative metabolomic characterisation identifies altered portal vein serum metabolome contributing to human hepatocellular carcinoma. *Gut*. 2022;71(6):1203–1213.
38 Virtanen P, Gommers R, Oliphant TE, et al. SciPy 1.0: fundamental algorithms for scientific computing in Python. *Nat Methods*. 2020;17(3):261–272.
39 Yu W, Wu B, Lin N, Stone K, Williams K, Zhao H. Detecting and aligning peaks in mass spectrometry data with applications to MALDI. *Comput Biol Chem*. 2006;30(1):27–38.
40 Yang J, Zhao X, Lu X, Lin X, Xu G. A data preprocessing strategy for metabolomics to reduce the mask effect in data analysis. *Front Mol Biosci*. 2015;2:4.
41 Liu W, Luo Y, Dai J, et al. Monitoring retinoblastoma by machine learning of aqueous humor metabolic fingerprinting. *Small Methods*. 2022;6(1):e2101220.
42 Wishart DS, Guo A, Oler E, et al. HMDB 5.0: the human metabolome database for 2022. *Nucleic Acids Res*. 2022;50(D1):D622–D631.
43 Pedregosa F, Varoquaux G, Gramfort A, et al. Scikit-learn: machine learning in Python. *J Mach Learn Res*. 2012;12:2825–2830.
44 Sun X, Xu W. Fast implementation of DeLong's algorithm for comparing the areas under correlated receiver operating characteristic curves. *ISPL*. 2014;21(11):1389–1393.
45 DeLong ER, DeLong DM, Clarke-Pearson DL. Comparing the areas under two or more correlated receiver operating characteristic curves: a nonparametric approach. *Biometrics*. 1988;44(3):837–845.
46 Mcinnes L, Healy J. UMAP: uniform manifold approximation and projection for dimension reduction. *J Open Sour Software*. 2018;3(29):861.
47 Pang Z, Chong J, Zhou G, et al. MetaboAnalyst 5.0: narrowing the gap between raw spectra and functional insights. *Nucleic Acids Res*. 2021;49(W1):W388–W396.
48 Warton DI, Wright ST, Wang Y. Distance-based multivariate analyses confound location and dispersion effects. *Methods Ecol Evol*. 2011;3(1):89–101.
49 Wei YF, Ning L, Xu YL, et al. Worldwide patterns and trends in ovarian cancer incidence by histological subtype: a population-based analysis from 1988 to 2017. *EClinicalMedicine*. 2025;79:102983.
50 Hilvo M, de Santiago I, Gopalacharyulu P, et al. Accumulated metabolites of hydroxybutyric acid serve as diagnostic and prognostic biomarkers of ovarian high-grade serous carcinomas. *Cancer Res*. 2016;76(4):796–804.
51 Lopez-Otin C, Pietrocola F, Roiz-Valle D, Galluzzi L, Kroemer G. Meta-hallmarks of aging and cancer. *Cell Metab*. 2023;35(1):12–35.
52 Zou H, Hastie T. Regularization and variable selection via the elastic net. *J R Stat Soc B*. 2005;67(2):301–320.
53 Xiao Y, Ma D, Yang YS, et al. Comprehensive metabolomics expands precision medicine for triple-negative breast cancer. *Cell Res*. 2022;32(5):477–490.
54 Pan J, Hu Y, Sun S, et al. Glycoproteomics-based signatures for tumor subtyping and clinical outcome prediction of high-grade serous ovarian cancer. *Nat Commun*. 2020;11(1):6139.
55 Chowdhury S, Kennedy JJ, Ivey RG, et al. Proteogenomic analysis of chemo-refractory high-grade serous ovarian cancer. *Cell*. 2023;186(16):3476–3498.
56 Pavlidis N, Rassy E, Vermorken JB, et al. The outcome of patients with serous papillary peritoneal cancer, fallopian tube cancer, and epithelial ovarian cancer by treatment eras: 27 years data from the SEER registry. *Cancer Epidemiol*. 2021;75:102045.
57 Ghose A, McCann L, Makker S, et al. Diagnostic biomarkers in ovarian cancer: advances beyond CA125 and HE4. *Ther Adv Med Oncol*. 2024;16:17588359241233225.
58 Wu S, Xu K, Chen G, Zhang J, Liu Z, Xie X. Identification of serum biomarkers for ovarian cancer using MALDI-TOF-MS combined with magnetic beads. *Int J Clin Oncol*. 2012;17(2):89–95.
59 Shah S, Cheung A, Kutka M, Sheriff M, Boussios S. Epithelial ovarian cancer: providing evidence of predisposition genes. *Int J Environ Res Public Health*. 2022;19(13):8113.
60 Li J, Wang Z, Liu W, et al. Identification of metabolic biomarkers for diagnosis of epithelial ovarian cancer using internal extraction electrospray ionization mass spectrometry (iEESI-MS). *Cancer Biomark*. 2023;37(2):67–84.
61 Wang X, Zhao X, Zhao J, Yang T, Zhang F, Liu L. Serum metabolite signatures of epithelial ovarian cancer based on targeted metabolomics. *Clin Chim Acta*. 2021;518:59–69.
62 Buas MF, Drescher CW, Urban N, et al. Quantitative global lipidomics analysis of patients with ovarian cancer versus benign adnexal mass. *Sci Rep*. 2021;11(1):18156.
63 Ahn HS, Yeom J, Yu J, Kwon YI, Kim JH, Kim K. Convergence of plasma metabolomics and proteomics analysis to discover signatures of high-grade serous ovarian cancer. *Cancers*. 2020;12(11):3447.
64 Buas MF, Gu H, Djukovic D, et al. Identification of novel candidate plasma metabolite biomarkers for distinguishing serous ovarian carcinoma and benign serous ovarian tumors. *Gynecol Oncol*. 2016;140(1):138–144.
65 Li Z, Wang C, Wang Z, et al. Allele-selective lowering of mutant HTT protein by HTT-LC3 linker compounds. *Nature*. 2019;575(7781):203–209.
66 Chong J, Wishart DS, Xia J. Using MetaboAnalyst 4.0 for comprehensive and integrative metabolomics data analysis. *Curr Protoc Bioinf*. 2019;68(1):e86.
67 Cao J, Yao QJ, Wu J, et al. Deciphering the metabolic heterogeneity of hematopoietic stem cells with single-cell resolution. *Cell Metab*. 2024;36(1):209–221.
68 Chen W, Yu H, Hao Y, et al. Comprehensive metabolic fingerprints characterize neuromyelitis optica spectrum disorder by

nanoparticle-enhanced laser desorption/ionization mass spectrometry. *ACS Nano*. 2023;17(20):19779–19792.
69 Wang R, Yang S, Wang M, et al. A sustainable approach to universal metabolic cancer diagnosis. *Nat Sustain*. 2024;7(5):602–615.
70 Sato S, Dyar KA, Treebak JT, et al. Atlas of exercise metabolism reveals time-dependent signatures of metabolic homeostasis. *Cell Metab*. 2022;34(2):329–345.
71 Havrilesky LJ, Dinan M, Sfakianos GP, et al. Costs, effectiveness, and workload impact of management strategies for women with an adnexal mass. *J Natl Cancer Inst*. 2015;107(1):322.
72 Menon U, McGuire AJ, Raikou M, et al. The cost-effectiveness of screening for ovarian cancer: results from the UK collaborative trial of ovarian cancer screening (UKCTOCS). *Br J Cancer*. 2017;117(5):619–627.
73 Wang Y, Stancliffe E, Fowle-Grider R, et al. Saturation of the mitochondrial NADH shuttles drives aerobic glycolysis in proliferating cells. *Mol Cell*. 2022;82(17):3270–3283.
74 Reinfeld BI, Madden MZ, Wolf MM, et al. Cell-programmed nutrient partitioning in the tumour microenvironment. *Nature*. 2021;593(7858):282–288.
75 Kanarek N, Keys HR, Cantor JR, et al. Histidine catabolism is a major determinant of methotrexate sensitivity. *Nature*. 2018;559(7715):632–636.
76 Park Y, Han Y, Kim D, et al. Impact of exogenous treatment with histidine on hepatocellular carcinoma cells. *Cancers*. 2022;14(5):1205.
77 Sud M, Fahy E, Cotter D, et al. Metabolomics workbench: an international repository for metabolomics data and metadata, metabolite standards, protocols, tutorials and training, and analysis tools. *Nucleic Acids Res*. 2016;44(D1):D463–D470.